Pair and multi-particle dispersion in numerical simulations of convective boundary layer turbulence

I. M. Mazzitelli, F. Fornarelli, A. S. Lanotte, and P. Oresta

Citation: Physics of Fluids (1994-present) **26**, 055110 (2014); doi: 10.1063/1.4878318
View online: http://dx.doi.org/10.1063/1.4878318
View Table of Contents: http://scitation.aip.org/content/aip/journal/pof2/26/5?ver=pdfcov
Published by the AIP Publishing

PHYSICS OF FLUIDS **26**, 055110 (2014)

Pair and multi-particle dispersion in numerical simulations of convective boundary layer turbulence

I. M. Mazzitelli,[1] F. Fornarelli,[1] A. S. Lanotte,[2,a)] and P. Oresta[1,3]
[1]*Department of Engineering for Innovation, University of Salento, and INFN Sez. Lecce, 73100 Lecce, Italy*
[2]*CNR-ISAC and INFN, Sez. Lecce, 73100 Lecce, Italy*
[3]*Department of Mathematics, Mechanics and Management, Polytechnic of Bari, 70126 Bari, Italy*

(Received 10 August 2013; accepted 6 May 2014; published online 27 May 2014)

Tracer dispersion within a highly convective planetary boundary layer is studied by means of a large-eddy simulation (LES) model for the continuous phases describing the temperature and velocity fields, and with the Lagrangian tracking of particle trajectories. Particle velocities are decomposed into their resolved and unresolved (or sub-grid) components. The former are evaluated by interpolation from the LES velocity field, the latter are given by a Lagrangian kinematic model that correctly describes the turbulent dispersion of clouds of particles. It is shown that, thanks to the Lagrangian sub-grid model, a clear inertial range is detectable in the time domain. In this range, particle separation grows according to Richardson's law, and nicely compares with previous experimental and numerical measurements. The collective motion of four particles, initially located at the vertices of regular tetrahedra, is also studied. The evolution of tetrad shape and orientation is contrasted with those obtained in homogeneous and isotropic flows. Results show that an agreement is achieved at small time lags. At larger times, the boundary layer reveals its anisotropic structure and the tetrad shape statistics deviate from results obtained in ideal flows.
 [http://dx.doi.org/10.1063/1.4878318]

I. INTRODUCTION

Warm cloud formation, bubbly convective flows, pollutant dispersion in the atmosphere are instances of phenomena governed by the turbulent nature of the advecting flow, and where a continuous phase coexists with a discrete one.[1–3] The simplest case is when the discrete phase is due to small, neutrally buoyant tracer particles – i.e., following fluid streamlines – seeding a statistically isotropic and homogeneous turbulent (HIT) flow. In such a case, the Eulerian statistics interfaces with the Lagrangian statistics of turbulence: from the Eulerian point of view, we can study the diffusion of scalar-field fluctuations, but more naturally from the Lagrangian point of view, we can study tracer pair[4] or multiparticle dispersion.[5,6]

Tracer pair dispersion in HIT is widely studied both experimentally and numerically (see Sawford,[7] and Salazar and Collins[8] for two recent reviews on the topic). The theoretical basis for these studies was put by Richardson in 1926 in a seminal work,[9] by observing the way balloons separate in the atmosphere, well before the contribution of Kolmogorov and Obukhov on scalar turbulence.[10]

Despite the elapsed time, experimental studies[11–13] on Lagrangian turbulence have not been as numerous as those in the Eulerian reference frame, because of the difficulties in obtaining long, high frequency records of Lagrangian trajectories in fully developed turbulent flows at moderate to high Reynolds numbers. Recent technological improvements in recording high frequency, high resolution

a)Author to whom correspondence should be addressed. Electronic mail: a.lanotte@isac.cnr.it

data have however renewed the interest in the topic, and there are now a number of laboratory studies focusing either on single tracer statistics,[14] and on pair[15,16] or multi-particle dispersion.[17,18] Often at comparable Reynolds number, a large amount of direct numerical simulations (DNS) studies have been performed focusing on Lagrangian particle dispersion in two-dimensional and three-dimensional homogeneous and isotropic flows,[19–22] also in the case of inertial particles,[23] or in anisotropic and/or inhomogeneous flows.[24,25]

In brief, Richardson's theory for pair dispersion in HIT states that given a pair of tracers – of position vector $\mathbf{x}_1(t)$ and $\mathbf{x}_2(t) = \mathbf{x}_1(t) + \mathbf{r}(t)$, respectively – having at time t_0 a small separation r_0, the probability to observe at a later time $t > t_0$ a pair separation $r > r_0$ depends on the amplitude r only. Asymptotically, the probability density function (PDF) $p(r, t|r_0, t_0)$ is also expected to become independent of the initial conditions, i.e., $p(r, t|r_0, t_0) = p(r, t)$ for $t \gg t_0$ and $r \gg r_0$. Richardson[9] also derived the shape of this PDF, which is non-Gaussian but self-similar,

$$p(r,t) \simeq \frac{r^2}{\langle r^2(t)\rangle^{3/2}} \exp\left(-B\frac{r^2}{\langle r^2(t)\rangle}\right)^{1/3}, \tag{1}$$

where B is a dimensionless constant. Richardson's[9] approach is *exact* for a self-similar velocity field, with no temporal correlations.[5,26] Both these hypotheses are not verified for real turbulent flows, and very recently their validity has been questioned in experiments[16,28] and in numerical studies.[27,29,30] Nevertheless, Richardson's[9] approach represents the theoretical basis to study dispersion, and moreover it gives predictions which are to some extent valid.[20,21,27]

The goal of this paper is to contribute to the understanding of the relative motion of *pairs* and *clouds* of particles in a turbulent flow, generated by atmospheric convection. The atmospheric convective boundary layer is a well studied instance of strongly anisotropic and inhomogeneous flow,[31–33] whose dynamics and statistics are governed by turbulence generated both by thermal and mechanical effects, due to convection and shear, respectively. Relative dispersion in non-ideal flows has been considered in observational studies in both the atmosphere and the ocean (see, e.g., LaCasce[34]). Results[35] consistent with Richardson's[9] 1926 observations have been found for balloon separations in the range of scales of 100 km $\leq r \leq$ 1000 km.

Here, the focus is on much shorter scales $r \leq 1$ km, since we deal with the atmospheric convective boundary layer. The setup of our dispersion study reproduces that of classical laboratory,[36,37] and numerical experiments,[38–40] which consider a scalar emission from an instantaneous line source. To study tracer dispersion in the CBL, we carried out a numerical study, described in Sec. II, by means of a large-eddy simulation (LES) model for the Eulerian velocity and temperature fields,[33,41–45] complemented by the Lagrangian tracking of thousands of tracer particles. The particle velocity is obtained by a superposition of two contributions: the first results from the LES velocity field; the second from a sub-grid scale (SGS) kinematic model,[46] that correctly reproduces the dispersion statistics of pairs and groups of tracers, in homogeneous and isotropic turbulence. In Sec. III, pair dispersion is studied in terms of the separation and relative velocity statistics: as already highlighted in ideal flows,[20,21] the intermittent nature of Eulerian velocity fluctuations leaves its signature on the moments of Lagrangian separations and relative velocities of pairs of tracers.

More insights on Lagrangian turbulence comes from the evolution of four particles organized in tetrahedra, described in Sec. IV. The tetrads change their initial geometrical properties, such as shape and size, depending on the local turbulence.[47,48] We contrast the temporal evolution of the tetrads in a CBL, with numerical and analytical results obtained in statistically isotropic turbulence.[48–50] In particular we show that, at large times, the anisotropy and inhomogeneity of the CBL lead to different shape and orientation statistics with respect to homogeneous and isotropic turbulence. In the CBL, tetrads slow down their tendency to form elongated volumes, and rotate until their longer axis lies parallel to the ground. We are not aware of measurements of pair separation PDF and tetrad statistics in the three-dimensional atmospheric boundary layer turbulence, hence these measurements will be compared to analogous results in homogeneous and isotropic turbulence, or to laboratory experiments of Rayleigh-Bénard convection, when possible. A summary of the work is in Sec. V.

II. THE EULERIAN-LAGRANGIAN MODEL

A. The large-eddy simulation for the convective boundary layer

The convective boundary layer evolves according to the Navier-Stokes equations, with temperature coupling via the Boussinesq approximation, and according to the continuity equation. The temperature field is described by an advection-diffusion equation. The temporal evolution of the velocity and potential temperature is achieved by means of the large-eddy simulation model extensively described in Lanotte and Mazzitelli,[33] that is based on the LES model of Moeng.[43] The LES code computes the velocity $\mathbf{u}$, temperature θ, and pressure p on a computational grid, resolving motions on scales larger than a filter scale Δ, which is of the order of the grid size. Fluctuations of the fields on smaller (or sub-grid) scales are modeled in terms of their values on the resolved scales, by applying the dynamic eddy-viscosity model proposed by Germano and co-workers.[51] In addition, the code integrates a model equation for the sub-grid scale kinetic energy e. For details on the equations of motions, on their numerical integration, and on the SGS closures, we refer to Moeng[43] and to Lanotte and Mazzitelli.[33]

In the present work, the physical domain has dimensions $L_x = L_y = 5000$ m in the wind and crosswind directions, and $L_z = 2000$ m in the vertical-gravity g-direction. The grid is composed of 128^3 mesh points, yielding a resolution $\Delta x = \Delta y \simeq 39$ m and $\Delta z \simeq 16$ m. The boundary layer is forced by the homogeneous, constant in time, surface temperature flux $H_0 = 0.24$ K m/s and by the constant geostrophic wind $(U_{gx}, U_{gy}) = (3.5\text{m/s}, 0)$. The initial boundary layer height is $z_{0i} \sim 1200$ m, the inversion strength in the entrainment zone $S = 0.05$ K/m, and the free atmosphere lapse rate $\Gamma_{fa} = 0.003$ K/m.

The relevant parameters of the convective boundary layer are collected in Table I.

B. The Lagrangian simulation

The Lagrangian particle velocity is computed according to

$$\mathbf{v}(\mathbf{x}(t)) = \mathbf{u}(\mathbf{x}(t), t) + \mathbf{u}'(\mathbf{x}(t), t)\,, \tag{2}$$

where $\mathbf{u}(\mathbf{x}, t)$ is the LES resolved velocity, evaluated by a trilinear interpolation of the Eulerian velocity field at the particle position $\mathbf{x}(t)$, and $\mathbf{u}'$ is a sub-grid scale term, prescribed according to the kinematic model detailed in Mazzitelli *et al.*[46] The unresolved, fluctuating term $\mathbf{u}'$ reflects the location of the particle: close Lagrangian neighbours have spatially correlated velocity fluctuations. In brief, a multiscale, homogeneous, and isotropic velocity field is associated with each particle; the tracer field is such that neighbouring particles feel correlated velocities having Kolmogorov like space-time scaling properties for the inertial range of $3D$ turbulent cascade.[52] Hence, for the relative dispersion statistics, a scaling behavior indicative of the inertial range of scales is obtained.[46] Intermittency and non-Gaussian corrections are excluded. The Lagrangian sub-grid scale (LSGS) model is suitable to assess single-point, two-point, as well as multi-point turbulent statistics in homogeneous and isotropic turbulence.

The single particle velocity field has three independent components, and each of them is made up of the superposition of N_m modes, defined on logarithmically equally spaced shells $l_n = L_0/\rho^n$ with

TABLE I. Large-eddy simulation parameters. The symbols indicate: L_i, $i = x, y, z$ the dimensions of the physical domain; U the intensity of the mean wind along x direction in the mixed layer; z_0 the roughness length; z_i the boundary layer height; z_i/L, with L the Obukhov length, the stability parameter; the convective velocity $\omega_* = (g z_i H_0/\theta_0)^{1/3}$, with $H_0 = 0.24$ K m/s the surface temperature flux and $\theta_0 = 286.75$ K a reference temperature; the convective time scale $\tau_* = z_i/\omega_*$. Variables U, z_i, z_i/L, ω_* are temporal averages for $6 < t/\tau_* < 11.5$. Note that $|z_i/L| \gg 10$ indicates a regime of strong convection. In a CBL, z_i, ω_*, and τ_* are the turbulent integral length, velocity, and time scales, respectively.

L_x, L_y (m)	L_z (m)	U (m s^{-1})	z_0 (m)	z_i (m)	z_i/L	ω_* (m/s)	τ_* (s)
5000	2000	3.2	0.1	1240	−140	2.17	572

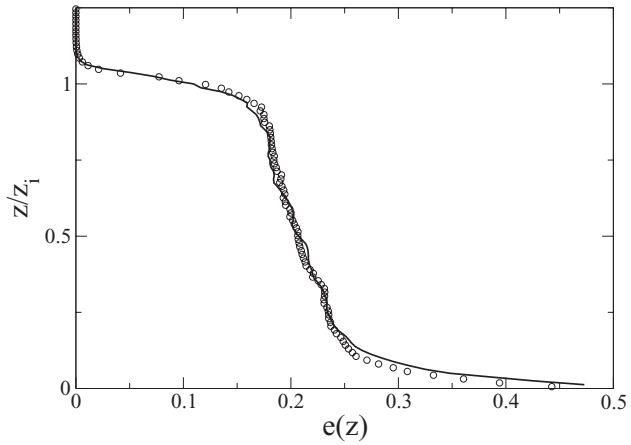

FIG. 1. A comparison of the kinematic model particle energy (circles) with the sub-grid scale turbulent kinetic energy computed by the LES. Time average is evaluated for $10 < t/\tau_* < 11.5$.

$n = 0, \ldots, N_m - 1$ and with the mode ratio ρ chosen as $\rho = 2^{1/4}$. The corresponding wavenumbers, velocities, and time-scales are

$$k_n = \frac{2\pi}{l_n}, \quad u_n = A_0\, k_n^{-1/3}, \quad \tau_n = \frac{l_n}{u_n}, \tag{3}$$

with $A_0 = \sqrt{2C_K}\varepsilon^{1/3}$. The turbulent modes at scale l_n decorrelate with the timescale τ_n, according to Ornstein-Uhlenbeck processes. In Eq. (3), ε is the mean kinetic energy dissipation, evaluated from the LES Eulerian fields in the mixing layer. The constant C_K is fixed by requiring that the sub-grid scale kinetic energy of the tracers is locally equal to the horizontally averaged SGS turbulent kinetic energy $e(z)$ derived from the LES model.

The amplitude of the sub-grid scale velocity fluctuation, to be substituted into Eq. (2), is modulated by the factor $\varepsilon(z)/\varepsilon$, with $\varepsilon(z)$ the z-dependent (horizontally averaged) kinetic energy dissipation. The modulating factor is updated during the numerical simulation every 200 time steps ($\simeq \tau_*/2$), since in a convective boundary layer only a quasi-steady state is obtained (note that the mean temperature is always increasing as well as the boundary layer height). Such a procedure offers two advantages: the first is to include in the LSGS kinematic model the dependence on the coordinate z of the sub-grid Eulerian turbulent kinetic energy; the second is to account for the growth in time of the turbulent zone (the mixed layer), due to the increase of the boundary layer height z_i. In Figure 1, the comparison of the vertical profile of the sub-grid scale kinetic energy from the LES equation with that of the Lagrangian tracers shows a very good agreement between the Eulerian and the Lagrangian measurements. Table II contains the parameters of the sub-grid scale models.

Tracer particles are introduced in the large-eddy simulation after about six large-scale eddy turnover times have elapsed from the beginning of the run, when the system has reached a quasi-stationary state and a mixed layer is developed.

TABLE II. Sub-grid scale models parameters. The symbols indicate: ε the space-time average of the kinetic energy dissipation; C_K the adimensional constant defining the sub-grid velocities amplitudes in the Lagrangian model (see text); N_m the total number of LSGS modes in the particle model; L_0 and l_{N_m-1} the largest and smallest length scales in the LSGS, respectively; τ_0 and τ_{N_m-1} the slowest and fastest LSGS time scales, respectively. Note that $L_0 = 2\Delta x$, where Δx is the horizontal grid spacing, and that the ratio of the simulation time step dt to the fastest time scale τ_{N_m-1} is $dt/\tau_{N_m-1} \simeq 1/7$.

ε (m^2/s^3)	C_K	N_m	L_0 (m)	l_{N_m-1} (m)	τ_0 (s)	τ_{N_m-1} (s)
0.0027	0.6615	28	78	0.7	210	9.3

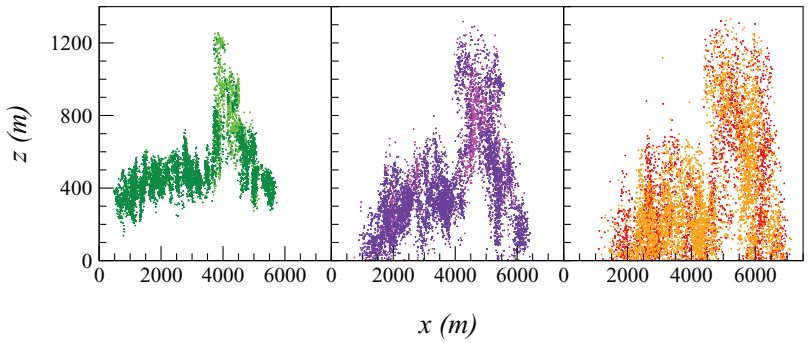

FIG. 2. A projection of particle distribution within a single simulation (with $N = 6656$ tracers) onto the $x - z$ plane, at time steps $t/\tau_* = 0.3$ (left), 0.6 (centre), and 1 (right). Particles in light shade colors lie within updrafts, while those in the dark color lie within downdrafts. At time $t = 0$, all tracers are located on horizontal planes at about $z_s \simeq 600$ m, the corresponding boundary layer height is $z_i \simeq 1200$ m.

Tracers are not constrained along the x and y directions, though their velocities are subject to the periodic boundary conditions. Along the gravity direction, reflection boundary conditions are imposed at the surface on both resolved and sub-grid velocities; whereas at the top of the boundary layer, particles are free to penetrate within and above the inversion zone. However, such event is very unlikely, owing to the weakness of turbulent agitation in the this stably stratified region.

With the setup described, Lagrangian tracking is performed for the tracers. Relative dispersion is studied by seeding the flow with $N = 6656$ passive particles, released in pairs with initial separation $r_0 \leq 1$ m. Pairs are initially distributed uniformly within an x elongated domain, of dimensions: $l_x \times l_y \times l_z \simeq 5000$ m $\times$ 40 m $\times$ 32 m, placed at a distance $z_s/z_i = 0.5$ from the surface. Their initial velocity equals that of the fluid at the particle position, plus the LSGS term.

Statistics are improved by ensemble averaging over 5 simulations that differ for the crosswind location of the domains where particle pairs are initially distributed. The projection of those domains onto the horizontal $x - y$ plane results in 5 rectangles separated by a distance, along the y direction, of 1 km from one another. The total number of pairs considered is therefore 16 640. In Fig. 2, a projection on the vertical $x - z$ plane of particle positions of a single run evolution is presented, at times $t/\tau_* = 0.3$, 0.6, and 1. From the snapshots, it appears that after about one large-scale eddy turn over time, tracers are spread within the whole boundary layer.

We note that in the case of LES with a coarse resolution, where statistical isotropy is hardly recovered at small scales, the present formulation of the LSGS model should be modified to include shear effects.

III. PAIR DISPERSION STATISTICS

Consider a cloud of particles, released at time $t = 0$, that move within a homogeneous and isotropic, incompressible velocity field, with Gaussian statistics and δ-correlated in time, such that the two-point longitudinal correlator $K(r, t) \equiv \langle[(\mathbf{u}(\mathbf{x} + \mathbf{r}, t) - \mathbf{u}(\mathbf{x}, t)) \cdot \hat{\mathbf{r}}]^2\rangle$ of the velocity field behaves as a power-law of the separation distance, $K(r) \propto r^{\xi}$, with $0 \leq \xi < 2$. The growth of the puff can be quantified in terms of the probability density function $p(\mathbf{r}, t)$ at time t for the separation vector $\mathbf{r}$ between two particles, chosen at random within the cloud. Upon the above hypothesis, the PDF exactly satisfies a Fokker-Planck equation that in spherical coordinates in three-dimensions reads as

$$\frac{\partial p(\mathbf{r}, t)}{\partial t} = \frac{1}{r^2} \frac{\partial}{\partial r} \left(r^2 \, K(r) \frac{\partial p(\mathbf{r}, t)}{\partial t} \right). \tag{4}$$

When the initial separation is sufficiently small and the travel time sufficiently large, a spherically symmetric solution of Eq. (4) exists (e.g., Monin and Yaglom,[10] p. 574): for $\xi = 4/3$, it has the shape given in Eq. (1).

Richardson's[9] empirical proposal states that the scalar eddy-diffusivity follows the so-called *four-thirds law*

$$K(r) = k_0 \varepsilon^{1/3} r^{4/3},$$

where k_0 is a dimensionless constant and ε the turbulent kinetic energy dissipation. By substituting such expression for $K(r)$, the large separation, long time solution of Eq. (4) is precisely

$$p(r,t) = \frac{Ar^2}{(k_0 \varepsilon^{1/3} t)^{9/2}} exp\left(-\frac{9\, r^{2/3}}{4\, k_0\, \varepsilon^{1/3} t}\right) \tag{5}$$

with $A = (3/2)^8/\Gamma(9/2)$. The second moment of this distribution is $\langle r^2(t)\rangle = \int_0^\infty r^2 p(r,t) dr$,

$$\langle r^2(t)\rangle = g \varepsilon t^3\,, \tag{6}$$

and the dimensionless constant $g = 1144\, k_0^3/81$ is considered universal.[20,21]

It is quite difficult to observe the scaling law (6) within DNS or laboratory experiments.[8] Indeed, as previously reported,[21] the pure superdiffusive behavior of (6) can be contaminated by both small and large scale cutoffs in the velocity field. Moreover, unless the initial separation r_0 is chosen very small, the scaling initially follows the so-called Batchelor regime, where the mean squared separation grows ballistically. As a result of these effects, spurious or mixed scaling behavior are observed, and a wide range of estimations of the constant g results. Alternatively, pair dispersion can be studied by means of *exit-time statistics*, in terms of the so-called Finite-Size Lyapunov exponent (FSLE).[53–55] Given the trajectories $\mathbf{x}_1(t)$ and $\mathbf{x}_2(t) = \mathbf{x}_1(t) + \mathbf{r}(t)$, FSLE is defined in terms of the average time $\langle T_\gamma(r)\rangle$ it takes for the distance $r = |\mathbf{r}|$ to grow by a factor $\gamma > 1$,

$$\lambda(r) = \frac{1}{\langle T_\gamma(r)\rangle} \ln \gamma\,. \tag{7}$$

At small scale, $r \to 0$, FSLE tends to the first characteristic Lyapunov exponent of the flow,[55] i.e., $\lambda(r) \to \lambda$. At larger scales, in the inertial range, where longitudinal Eulerian velocity fluctuations behave as $\langle[(\delta_r u)_\parallel]^2\rangle \simeq r^{2/3}$, the FSLE behaves as $\lambda(r) \simeq r^{-2/3}$. The FSLE reveals better the existence of scaling laws, since it samples pairs with comparable separations, thus avoiding contaminations from different regimes and limiting the impact of finite Reynolds effects.[21,58]

In the following, we first discuss, in Sec. III A, statistical measurements of relative dispersion obtained by fixing the time lag of observation, and then by fixing the spatial scale. In Sec. III B, we discuss the statistics of relative velocities along tracers pair trajectories.

A. Particle relative separation statistics

In a turbulent atmospheric boundary layer, the inertial range typically goes from scales of a few millimeters to scales of the order of 10^3 m. In the large-eddy simulations here presented, the cutoff length scale is of the order of $2\Delta x$, so, with a resolution of 128^3 grid points, the smallest resolved inertial range scale is $O(100$ m). As a consequence the LES presents about one decade of the Eulerian inertial range of spatial scales, and less for the Lagrangian inertial range of times, where finite Reynolds effects are known to be more critical.[56,57] However, the Lagrangian sub-grid scale model allows for an extension of the inertial range to much smaller time lags, down to τ_{N_m-1}.

Before considering pair statistics, it is mandatory to test that diffusion properties are not affected by the sub-grid model. To this aim, in Fig. 3, single particle diffusion is presented in terms of the mean square displacement with respect to the initial position $\mathbf{x}(0)$,

$$D(t) = \langle(\mathbf{x}(t) - \mathbf{x}(0))^2\rangle\,. \tag{8}$$

Results are shown for one set of large-eddy simulations, considering tracers trajectories obtained with and without the sub-grid scale Lagrangian model. The initial regime increases ballistically as t^2, which is expected in the inertial range of scale, whereas at large times $t \simeq 2\tau_*$ the Taylor diffusion begins. As expected, the sub-grid Lagrangian model does not modify single particle diffusion properties.

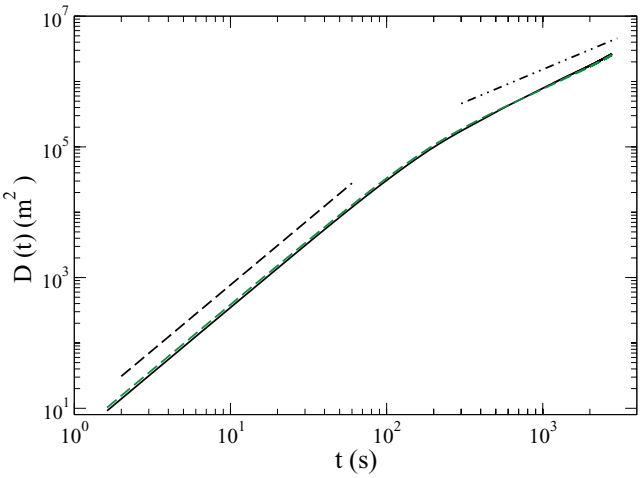

FIG. 3. Absolute diffusion for a numerical simulation with (dashed green line) and without (continuous black line) sub-grid scale Lagrangian model. The straight lines indicate, respectively, the ballistic $D(t) \propto t^2$ (dashed line) and linear diffusive $D(t) \propto t$ (dashed dotted line) scalings.

On the other hand, particle relative dispersion is largely affected by the presence of the SGS Lagrangian model. In Figure 4, a comparison is shown of relative dispersion second moment,

$$\langle r^2(t) \rangle = \langle (\mathbf{x}_2(t) - \mathbf{x}_1(t))^2 \rangle \,, \tag{9}$$

due to the LES velocity field only, and due to the LES plus Lagrangian SGS velocities. In the former case, pairs of tracers stay close to each other for about one large-scale eddy turn over time, before entering a regime of rapid separation. In contrast, in simulations with the LSGS, pairs rapidly forget their initial separation (Batchelor regime), and then separate super-diffusively with a scaling behavior very close to t^3.

To further analyze pair dispersion, we consider exit-time statistics. For this, we fix a set of thresholds, $r_n = \gamma^n r_0$, where $\gamma > 1$ and $n = 1, 2, 3, \ldots$ and then we measure the time, $T_\gamma(r_n)$, it takes for the pair separation to change from r_n to r_{n+1}. By averaging over the particle pairs ensemble, we obtain the mean exit time, $\langle T_\gamma(r_n) \rangle$, or mean *doubling time* if $\gamma = 2$. Figure 5 presents the inverse of the mean exit-time or FSLE, $\lambda(r)$, evaluated in numerical simulations with and without LSGS.

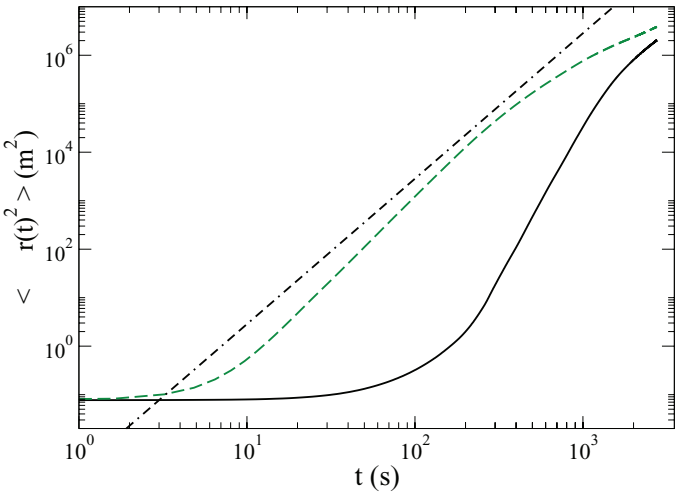

FIG. 4. Relative dispersion for simulations with (dashed, green line) and without (continuous black line) Lagrangian sub-grid scale model. The straight line indicates the Richardson regime, $\langle r^2(t) \rangle \propto t^3$.

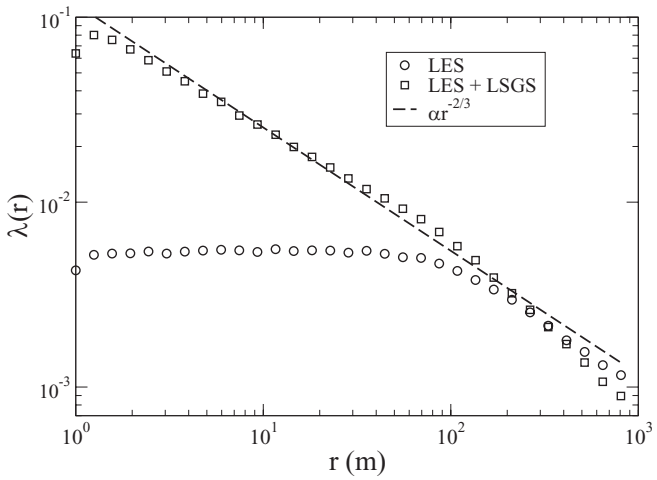

FIG. 5. Finite-size Lyapunov exponent for simulations with (squares) and without (circles) LSGS model. The straight line indicates the curve $\alpha r^{-2/3}$, with $\alpha = 0.12 \pm 0.01$, fitting the data in the inertial range of scales.

The growing factor is chosen as $\gamma = 1.25$. In the case where no LSGS is present, the expected Richardson scaling for the inertial range of turbulence $\lambda(r) \simeq r^{-2/3}$ starts only at scales of the order of $2\Delta x \simeq 100$ m, whereas at $r < 100$ m, the curve is flat: this is the signature of the lack of velocity correlations at smaller scales. In the simulation with LSGS, a well defined scaling region is evident, which extends down to scales $O(1\text{ m})$. We note that at separations of the order of the cutoff scale $r \simeq 2\Delta x$, the two FSLE curves are coincident, meaning that the sub-grid scale model recovers Lagrangian fluctuations of the resolved fields. Small discrepancies at larger separations are within statistical errors. A fit of the curve of the FSLE can be used to estimate the Richardson constant g of equation (6); indeed, following Boffetta and Sokolov,[20] an analytic expression of the mean exit-time can be derived from Richardson *exit-time* PDF, linking g with $\langle T_\gamma \rangle$,[20,21]

$$g = \frac{143}{81} \frac{(\gamma^{2/3} - 1)^3}{\gamma^2} \frac{r^2}{\varepsilon \langle T_\gamma(r) \rangle^3} . \tag{10}$$

The value so obtained in our LES is $g \simeq 0.27 \pm 0.07$, that belongs to the range of values reported in the literature [0.06 : 3.5], although it is smaller than the mostly agreed value $g \simeq 0.5$ found in three-dimensional HIT[12,20,21] and also in neutral boundary layer turbulence.[58] We stress however that in a recent laboratory study of turbulent thermal convection the Richardson constant has been found to be $g \sim 0.1$.[59] The evidence of a smaller value of the Richardson constant in turbulent convection also comes from a numerical study that found $g = 0.16$, attributing such value to the correlated motion of tracer pairs in thermal plumes.[60] These results point to the anisotropy of the pair dispersion process in convective turbulence.

To further analyze this observation, in Fig. 6 we present the decomposition of the total relative dispersion (9) for pairs with initial separation $r_0 = l_{N_m-1} \simeq 0.7$ m, into lateral and vertical components. The lateral dispersion is evaluated on the projection of the particle separation vector onto the horizontal planes, while the vertical one is evaluated with particle separation projected along the z direction. These plots are to be compared with those in Figure 2 of Ref. 59, where it is suggested that because of the vertical anisotropy, particle relative dispersion follows Richardson law if evaluated in the wall parallel planes.

We remark that the convective boundary layer differs from laboratory convection in a Rayleigh-Bénard cell, in that in the former case particles can penetrate within the entrainment zone at the top of the mixed layer, whereas in the latter they are vertically confined in the idealised convective cell. From Figure 6, it appears that on small time scales, the lateral and the vertical dispersion are similar, and are both close to Richardson law. This can be understood as follows: the inertial range of scales

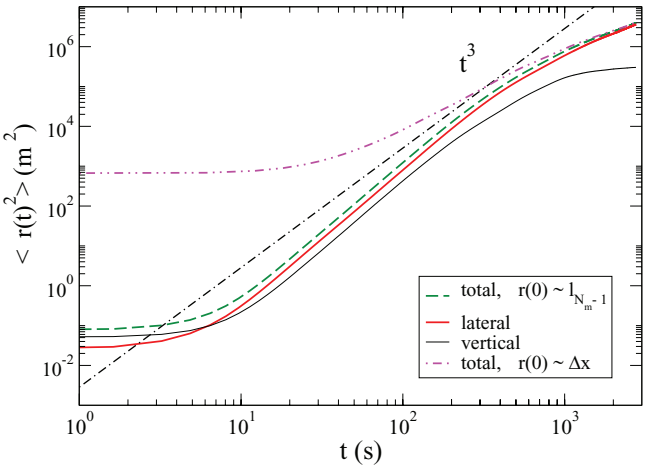

FIG. 6. Log-log plot of the total particle relative dispersion (green dashed), lateral dispersion (red solid bold), and vertical dispersion (solid black) for pairs whose initial separation is $r(0) = l_{N_m-1} \simeq 0.7$ m. The total relative dispersion (purple dashed-dotted) is also plotted for pairs whose initial separation is of the order of the grid-size in the horizontal plane, i.e., $r(0) = \Delta x \simeq 39$ m. The straight line (black dashed-dotted) is the Richardson regime, $\simeq t^3$.

is partly influenced by the sub-grid model statistics which is isotropic; moreover, in atmospheric flows, the inertial range is quite large, which allows for restoration of isotropy on the small scales.

We remark however that, on longer times yet belonging to the inertial range, as already found in Ref. 59, we also observe that the total dispersion is dominated by the lateral one, while vertical dispersion is strongly depleted. This is due to the vertical boundary constraints, making anisotropy dominant at those scales.

It is also interesting to look at the behavior of the relative dispersion second moment, at varying the initial separation of tracer pairs. Figure 6 contains the curve $\langle r^2(t)\rangle$, for pairs whose initial separation is of the order of the grid size, $r_0' = \Delta x \simeq 39$ m. Here, the LSGS scales play no role and an inertial range scaling is hardly present. At very large times, total relative dispersion curves coincide.

We now examine the statistical behavior of the separation probability density function $p(r, t)$. Results are shown in Figure 7, by plotting pair separation PDF evaluated at different times t. The time dependence is rescaled in terms of the second order moment, as done in Eq. (1). From time lags

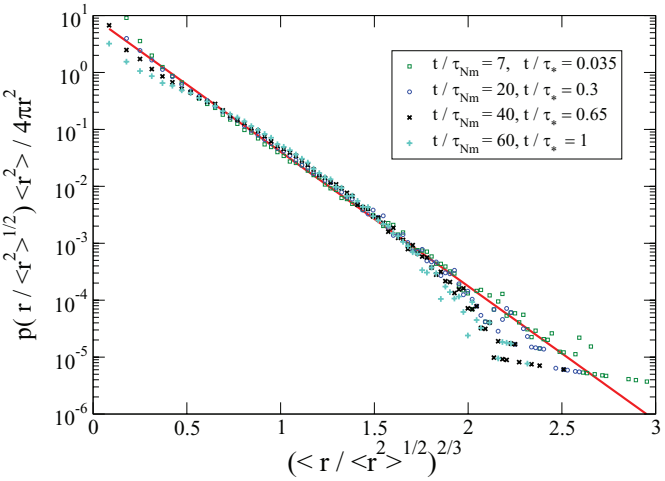

FIG. 7. Lin-log plot of the pair separation probability density function $p(r, t)$ at different times. Time dependency is rescaled in terms of the second order moment $\langle r^2(t)\rangle$. The straight line is Richardson's theoretical expectation.

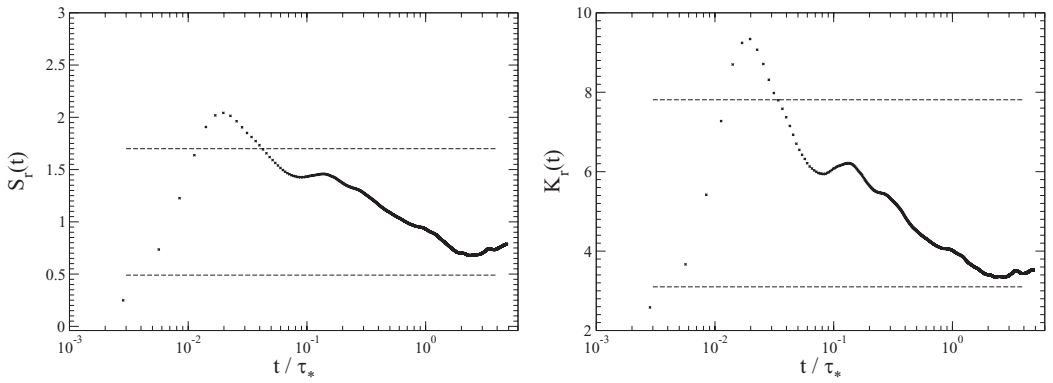

FIG. 8. Skewness (left) and kurtosis (right) of the particle separation distance, for pairs with initial separation $r_0 = l_{N_m-1}$. The straight lines indicate the following values of the skewness: 1.7 (Richardson value) and 0.49 (chi-squared value). The same for the kurtosis: 7.81 (Richardson value) and 3.1 (chi-squared value).

much smaller than the large-eddy turnover time τ_* until times $t \sim O(\tau_*)$, the pair separation PDF can be fitted by Richardson solution over a wide interval of spatial scales. Within the present statistics, comparable with those of recent experiments of HIT,[16] we can say that Richardson prediction for the pair separation PDF is well verified in CBL turbulence.

Additional analysis of the particle separation statistics is carried out by computing the skewness $S_r(t) = \langle [r(t) - \langle r(t) \rangle]^3 \rangle / [\sigma_r^2(t)]^{3/2}$ and the kurtosis $K_r(t) = \langle [r(t) - \langle r(t) \rangle]^4 \rangle / [\sigma_r^2(t)]^2$.

On a theoretical ground, the very existence of Eulerian intermittency tells us that pair dispersion cannot be described by a Fokker-Planck diffusive approach such as that of Eq. (4), which assumes temporal self-similarity in the dispersion process.

According to Richardson's model, the expected values in the inertial range for the skewness and the kurtosis are, respectively, 1.7 and 7.81. At larger scales, by assuming for $r^2(t)$ a chi-squared distribution with three degrees of freedom, these numbers should become 0.49 and 3.1. In Fig. 8, we compare theoretical expectations with results obtained in the LES runs with the use of the LSGS model. As reported in literature (see, e.g., Yeung and Borgas[61] and Biferale *et al.*[21]), the lack of a scaling regime where $S_r(t)$ and $K_r(t)$ are the fingerprint of the intermittent behavior of Lagrangian pair dispersion statistics. Here, we found that the deviations from Richardson's[9] expectations of the separation skewness and kurtosis at small time lags are much smaller than those observed in DNS or experiments: this comes as no surprise, since intermittent small-scale fluctuations of the velocity field are not present in the LSGS model. The small but detectable deviations that we observe are due to the interplay in the inertial range statistics of the LSGS velocities with the resolved ones.

Finally, the fact that they do not level off at the Richardson's[9] expectation values suggests contamination of the inertial range from the integral as well as from the small scales.

Before concluding this section, we present the temporal behavior of the maximum pair separation distance in Figure 9. Such quantity is evidently related to the maximum width reached by a small puff of a passive tracer released inside the mixed layer. The numerical evidence from the LES experiments is that the initial growth of the puff follows the power law $r_{max}^2 \propto t^{\gamma_1}$, with $\gamma_1 = 3$. Such behavior is limited to small times, when the puff dimension has not reached the boundary layer height z_i yet, and reproduces the behavior of the separation second moment $\langle r^2 \rangle$, thus exhibiting no anomalous effect. At larger times lags, still within the inertial range of time lags, the maximal separation grows slowly, and behaves as $r_{max}^2 \propto t^{\gamma_1}$, with $\gamma_2 = 2$. Recently, in Ref. 27 by means of DNS of homogeneous and isotropic turbulence, a similar quantity was measured, obtaining the behavior $r_c(t) \simeq t$. We attribute the observed difference to the fact that at small time lags, the Lagrangian statistics is in our case not affected by intermittent effects. Being an issue of possible practical interest, it would be very interesting to have an analytical derivation as well as measurements of this quantity from boundary layer experiments or direct numerical simulation of thermal convection. This is left for future work.

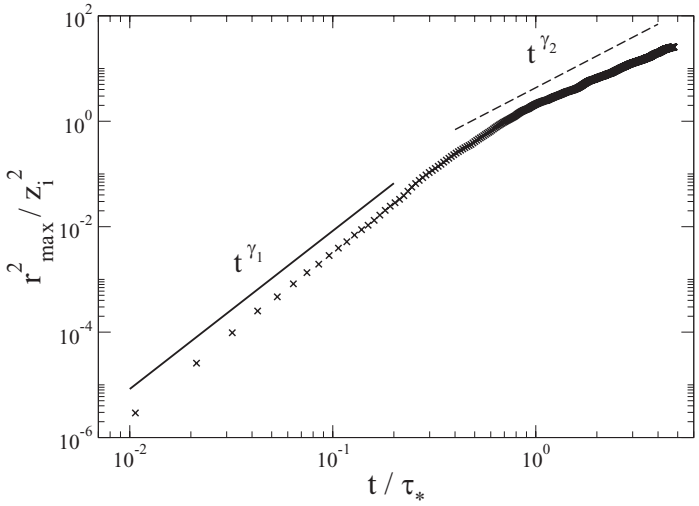

FIG. 9. The behavior of the maximum tracer pair separation distance squared r^2_{max}, normalised to the boundary layer height z_i, as a function of time t/τ_*. The straight lines have slopes $\gamma_1 = 3.0 \pm 0.2$ and $\gamma_2 = 2.0 \pm 0.2$.

B. Particle relative velocity statistics

The relative velocity of each tracer pair $\mathbf{v_r} \equiv \mathbf{v}_2(\mathbf{x}_2(t)) - \mathbf{v}_1(\mathbf{x}_1(t))$ is decomposed into its parallel (along separation direction) and normal components, according to

$$\mathbf{v_r} = v_p \hat{\mathbf{r}} + \mathbf{v}_n. \tag{11}$$

Here, $\hat{\mathbf{r}}$ is the unit vector in the direction of the separation, $\mathbf{r} = \mathbf{x}_2(t) - \mathbf{x}_1(t)$, v_p is the modulus of the parallel velocity component, and the vector $\mathbf{v}_n$ is the normal velocity component

$$v_p = \mathbf{v_r} \cdot \hat{\mathbf{r}}, \tag{12}$$

$$\mathbf{v}_n = \mathbf{v_r} - v_p \hat{\mathbf{r}}. \tag{13}$$

The probability density functions of v_p and of one component of $\mathbf{v}_n$ are measured and plotted in Fig. 10, together with a reference Gaussian function. The figure shows that the $p(v_p, t)$ is positively skewed, indicating that nearby particles are more likely to be diverging than converging at all times. The skewness decreases in time as the particle-pair PDF tends to the Gaussian function at large

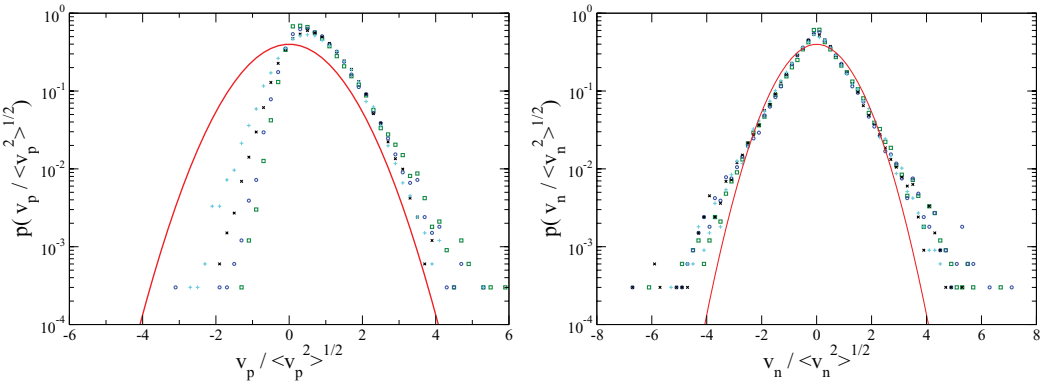

FIG. 10. The probability density functions of the parallel relative velocity component v_p (left) and one normal relative velocity component v_n (right), measured at different time lags, for pairs with initial separation $r_0 = l_{N_m-1}$. For comparison, a Gaussian function (red) is also plotted. For the symbols, see table in Figure 7.

times. In agreement with the small time lags isotropic statistics, $p(v_{n,z}, t)$ (z-component of $\mathbf{v}_n$) is symmetric, denoting that there is no preferred orientation of rotation around the separation axis. From both figures, important deviations from a normal behavior are observable, in agreement with similar results in DNS and experiments of homogeneous and isotropic turbulence.

IV. MULTI-PARTICLE STATISTICS: THE DISPERSION OF TETRAHEDRA

We consider tracer particles that are initially located at the four points of regular tetrahedra of side $d \simeq 0.15$ m, which implies that the side is smaller than the smallest length scale of the particle sub-grid velocity, $d < l_{N_m-1}$. The centre of mass of the tetrahedra are randomly distributed on the horizontal plane located at $z/z_i = 0.5$. Three simulations, equally spaced in time by about one large eddy-turnover-time τ_*, are carried out. Each simulation contains 4096 tetrads.

In order to display the tetrad shape evolution, the following change of coordinates is performed from the particle positions $\mathbf{x}_i$, $i = 1, \ldots, 4$ to the set $\boldsymbol{\rho}_i$, $i = 0, \ldots, 3$, defined as: $\boldsymbol{\rho}_0 = (\mathbf{x}_1 + \mathbf{x}_2 + \mathbf{x}_3 + \mathbf{x}_4)/2$, $\rho_1 = (\mathbf{x}_1 - \mathbf{x}_2)/\sqrt{2}$, $\rho_2 = (2\mathbf{x}_3 - \mathbf{x}_2 - \mathbf{x}_1)/\sqrt{6}$, $\rho_3 = (3\mathbf{x}_4 - \mathbf{x}_3 - \mathbf{x}_2 - \mathbf{x}_1)/\sqrt{12}$.[47] Owing to the homogeneity of the SGS velocity field and to the fact that tetrads initial distribution is on the plane $z/z_i = 0.5$ (that belongs to the homogeneous and isotropic region of the CBL), we expect that the statistics do not depend on the centre of mass $\boldsymbol{\rho}_0$, at least for times $t \leq \tau_*$. Therefore, we can repeat the analysis of tetrad statistics on the same path proposed for homogeneous and isotropic flows.[22,48,49] We define the square symmetric inertia matrix $\mathbf{I} = \rho\rho^T$, with column vectors ρ_i, $i = 1, 2, 3$. The matrix admits real positive eigenvalues, g_i, that can be ordered according to: $g_1 \geq g_2 \geq g_3$. The tetrahedron dimension is given by $r^2 = \frac{2}{3} tr(\mathbf{I}) = \frac{2}{3}(g_1 + g_2 + g_3)$ and the volume is $V = \frac{1}{3}\sqrt{det(\mathbf{I})} = \frac{1}{3}\sqrt{g_1 g_2 g_3}$. We also introduce the adimensional quantities $I_i = g_i/r^2$ (where $I_1 + I_2 + I_3 = 1$). For a regular tetrahedron, we should have $I_1 = I_2 = I_3 = 1/3$. If the four points are coplanar, the third index is null, $I_3 = 0$; while when the four points are aligned, both the second and third indices vanish, $I_2 = I_3 = 0$.

In Figure 11 (left plot), we present the temporal evolution of the mean eigenvalues of $\mathbf{I}$, together with the Richardson's prediction for the inertial range of separations, $\langle g_i \rangle \propto t^3$. We observe a nice agreement between the theory and the numerical results, due to the role of the LSGS.

As previously done for relative dispersion, we also assess fixed scale statistics to better disentangle scaling regimes. To this aim, we compute the average time $\langle T_\alpha(g_i) \rangle$ it takes for each eigenvalue g_i to increase its value of a factor $\alpha > 1$. On a dimensional ground, in agreement with Richardson's theory, we expect

$$\langle T_\alpha(g_i) \rangle \propto g_i^{1/3}. \tag{14}$$

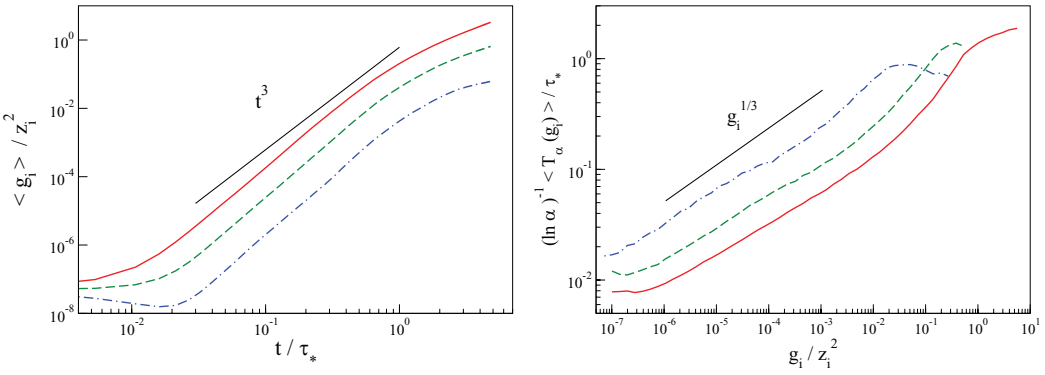

FIG. 11. (Left) The temporal behavior of the mean eigenvalues $\langle g_i \rangle$, with $i = 1$ (red-solid line) $i = 2$ (green dashed line), and $i = 3$ (blue dotted-dashed line). The continuous line is Richardson's expectation for the inertial range of scales. (Right) The exit-time measurements for the eigenvalues g_i. The dimensional expectation on the basis of the Richardson scaling regime is also shown for comparison (straight line).

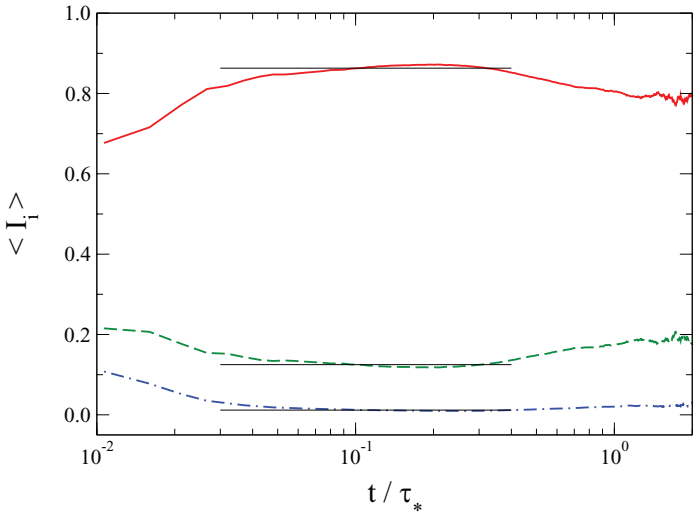

FIG. 12. Mean parameters $\langle I_i \rangle s$ evaluated on a subset of tetrahedra, with eigenvalues g_i belonging to the following ranges: $5 \times 10^{-7} < g_1/z_i^2 < 0.1$, $10^{-7} < g_2/z_i^2 < 0.01$, and $3 \times 10^{-7} < g_3/z_i^2 < 0.03$. The straight lines are best fit to the curves within the interval $t/\tau_* \in [0.03: 0.4]$. Here, $\langle I_1 \rangle = 0.863 \pm 0.007$, $\langle I_2 \rangle = 0.125 \pm 0.003$, and $\langle I_3 \rangle = 0.0118 \pm 0.0008$.

Results are plotted in Figure 11 (right plot), for the choice $\alpha = 1.4$. The observed behavior of the exit-time does not match exactly the theoretical prediction. Nevertheless, an inertial range can be identified where the slope of the curves is close to the Richardson expectation.

In Figure 12, the adimensional parameters $\langle I_i \rangle s$ are computed by selecting, at each time step, those tetrads where interparticle distances belong to the inertial range of scales. This is done on the basis of the exit-time measurements reported in Figure 11 (right plot) and corresponds to tetrads whose eigenvalues $g_i s$ are in the intervals $5 \times 10^{-7} < g_1/z_i^2 < 0.1$, $10^{-7} < g_2/z_i^2 < 0.01$, and $3 \times 10^{-7} < g_3/z_i^2 < 0.03$.

The best fit to the curves of Fig. 12, within the interval $t/\tau_* \in [0.03 : 0.4]$, are $\langle I_1 \rangle = 0.863 \pm 0.007$, $\langle I_2 \rangle = 0.125 \pm 0.003$, and $\langle I_3 \rangle = 0.0118 \pm 0.0008$, i.e., $\langle I_1 \rangle \gg \langle I_2 \rangle, \langle I_3 \rangle$. This indicates the dominance of very elongated tetrad structures. We remark that our results are consistent, within errorbars, with previous findings concerning homogeneous and isotropic turbulence, in Richardson-like model for tetrads dispersion,[50] where $\langle I_1 \rangle = 0.861$, $\langle I_2 \rangle = 0.128$, and $\langle I_3 \rangle = 0.011$, and they also agree with direct numerical simulations[48] results, where $\langle I_1 \rangle = 0.854$, $\langle I_2 \rangle = 0.135$, and $\langle I_3 \rangle = 0.011$.

The existence of a region where the tetrads are strongly stretched in one direction can be evidenced by computing the ratio $\langle v_p^2 \rangle / \langle v_n^2 \rangle$, where the parallel, v_p, and transversal, v_n, relative velocities, defined according to Eqs. (12) and (13), are the mean values over the 6 independent particle pairs of each tetrahedron. The brackets $\langle \cdot \rangle$ indicate an average over all tetrahedra. Fig. 13 shows that for $t/\tau_* \leq 1$ the ratio is larger than one, indicating that separation between particles dominates over rotation. The maximum is achieved at $t/\tau_* \simeq 0.03$, followed by a slight descent. A steeper descent begins at $t/\tau_* \simeq 0.3 - 0.4$. Two possibilities are here explored in order to shed light on the transition point between these two distinct regimes.

First, it may be attributed to inhomogeneous effects due to particles' collective motion towards the bottom zone of the boundary layer, that is shown in Fig. 14, where the distribution of the tetrad centres of mass is plotted as a function of the vertical coordinate z and of time t. From the plot we infer that, at time $t/\tau_* \sim 0.4$, a large number of tetrads has already moved close to the ground, where boundary effects prevail.

However, by selecting those tetrads whose centre of mass remains, at all times, in the region $z/z_i \in [0.4 : 0.6]$, we do not observe different behaviors. This indicates that the anisotropies are more likely connected with the mixed layer structures, rather than with the bottom boundary constraints.

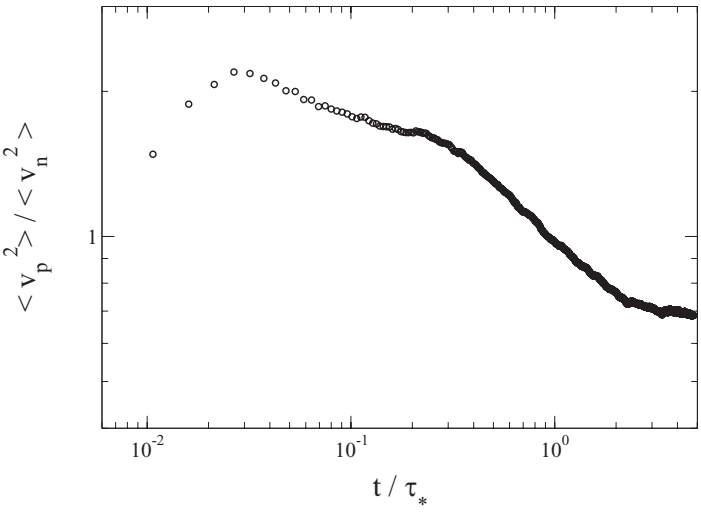

FIG. 13. Ratio of the squared velocity difference along separation direction, v_p^2, to the squared transversal component, v_n^2. v_p^2 and v_n^2 are the mean relative velocities between the 6 particle couples of each tetrahedron. The brackets $\langle \cdot \rangle$ indicate average over all tetrads.

Second, we consider the influence of the sub-grid scale model by computing the ratio of the largest model time scale τ_0 (see Table II) to the LES convective time τ_* (see Table I), that is, $\tau_0/\tau_* \simeq 0.36$. Whether the kinematic model is dominant or not is investigated by looking at the relative contributions to the particle velocity difference resulting from the LES and from the sub-grid model. Figure 15 shows that, up to times $t/\tau_* \sim 0.2$, the main contribution comes from the sub-grid scale model. At later times, the resolved component becomes more important.

To summarise, the transition between the different regimes in tetrad shape evolution can be attributed to the presence of BL structures, i.e., the plumes, leading to deviations from analogous results in HIT and from Richardson scaling. In the CBL, we measure the presence of less elongated but flatter structures.

For completeness, we remark that the time scale τ_0 is calculated through the largest model length, L_0, the fluid energy dissipation, ε, and the model constant C_K, all parameters dependent on the large-eddy simulation of the CBL. By changing the large-eddy simulation resolution, we do not expect to measure large deviations from the present case. The qualitative trend will be the same, i.e., an homogeneous and isotropic turbulent-like regime followed by an anisotropic plume-dominated

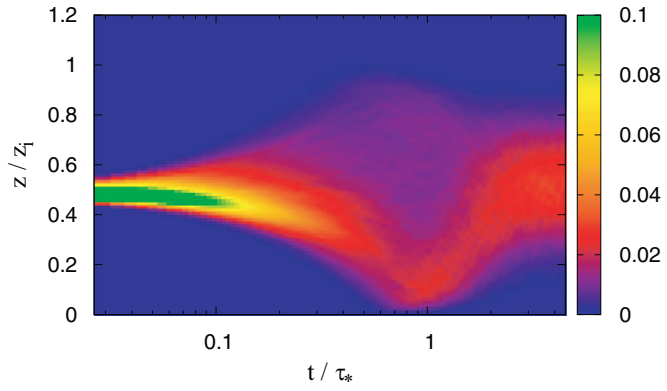

FIG. 14. Distribution of the tetrads as a function of the normalized surface distance z/z_i and of time t/τ_*. We plot the fraction of tetrads, with respect to the total number, whose centre of mass is located at time (t) at height (z).

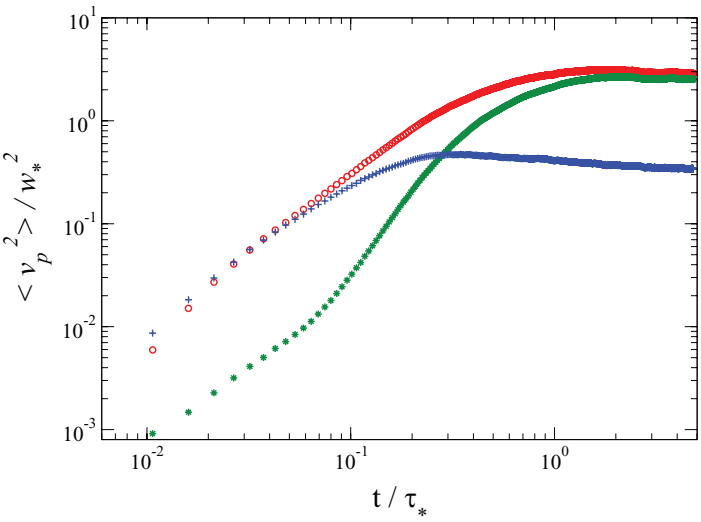

FIG. 15. Mean-squared relative velocity projected along the separation direction. Total velocity (red circles), sub-grid scale component (blue pluses), LES velocity component (green stars).

situation, separated by a cutoff time scale $t_c/\tau_* \sim O(10^{-1})$. The quantitative analysis of t_c is left for future studies.

Finally, we comment on the orientation of the tetrahedra within the CBL by looking at the direction of the eigenvectors of the inertia matrix $\mathbf{I}$. We measure that, for $t/\tau_* \leq 0.4$, the tetrads do not display any preferential orientation; at larger times, the eigenvector relative to the largest eigenvalue I_1 rotates until lying in the horizontal plane (not shown). This may be easily justified by considering that the boundary constraints on the particles allow for stretching of the tetrahedron only on this plane.

V. CONCLUSIONS

We carried out a set of large-eddy numerical simulations of a turbulent convective boundary layer, seeded with thousands of tracer particles. The Lagrangian statistics of turbulence are investigated by the time evolution of particle pairs and tetrads. The velocity fluctuations at small scales are modelled for both the continuous Eulerian phase and for the Lagrangian particles. The Lagrangian particle sub-grid model does not modify LES results concerning single particle dispersion. On the other hand, particle relative dispersion is completely reshaped by the LSGS model. In simulations without the Lagrangian sub-grid scale model, particles within a pair stay together for quite a long time, before entering a regime of rapid separation. In simulations with LSGS, the tracer pairs immediately start to separate and relative dispersion reaches a scaling behavior close to the Richardson scaling regime $\simeq t^3$.

In agreement with recent numerical and laboratory experiments of turbulent thermal convection, we observe a reduced value of the Richardson constant g, in comparison to homogeneous and isotropic turbulence. We explain this result as a consequence of the anisotropy induced by the tracer motions in the thermal plumes.

We examined pair and tetrad separation statistics looking at the behavior at fixed scales also. This was done in order to enforce the statement of an extended Richardson regime, thanks to the Lagrangian sub-grid model.

The relative velocity of particle pairs is decomposed into its parallel v_p (along separation direction) and normal $\mathbf{v_n}$ components. The probability density function $p(v_p, t)$ is positively skewed, pointing out that nearby particles are more likely to be diverging than converging at all times. The skewness decreases in time and particles velocity distribution tends to a Gaussian function at large

times. The distribution $p(v_n, t)$ is symmetric, denoting no preferred direction of v_n. The result is consistent with isotropy of turbulence on the inertial scales.

The statistics of tetrads – computed for the first time in the atmospheric boundary layer – show the dominance of very elongated structures. Here also, the Lagrangian sub-grid scale model plays a key role, enabling the observation of an extended inertial range scaling regime.

A time dependent transition occurs making a sharp difference between two distinct regimes: an homogeneous and isotropic turbulence-like regime and an anisotropic, plume-dominated one. The anisotropies are more likely connected with the mixed layer structures, rather than with the bottom boundary constraints. The transition between different regimes can also be attributed to the different features presented by the LES velocity field with respect to the sub-grid scale homogeneous and isotropic one. Indeed, the presence of boundary-layer structures, i.e., the plumes, leads to deviations from Richardson scaling and to the observation of less elongated but flatter structures.

The results presented in this work on pair and multiparticle dispersion are expected to be observed, within the limitations of the numerical model, in all highly convective boundary layers, characterised by a well extended mixed layer region and the presence of strong thermal structures.

ACKNOWLEDGMENTS

We thank F. Toschi, B. J. Devenish, and G. Lacorata for useful discussions. I.M.M, F.F., and P.O. gratefully acknowledge support by MIUR-FIRB under Grant No. RBFR08QIP5_001. We acknowledge the CINECA award within the ISCRA-B project "CLOUD" under the ISCRA initiative, for the availability of high performance computing resources and support. We thank F. Grasso for technical assistance on Cluster Zeus at CNR ISAC, U.O.S. Lecce (Italy).

[1] R. A. Shaw, "Particle-turbulence interactions in atmospheric clouds," Annu. Rev. Fluid Mech. **35**, 183–227 (2003).
[2] R. Lakkaraju, R. J. A. M. Stevens, P. Oresta, R. Verzicco, D. Lohse, and A. Prosperetti, "Heat transport in bubbling turbulent convection," Proc. Natl. Acad. Sci. U.S.A. **110**(23), 9237–9242 (2013).
[3] A. Stohl, M. Hittenberger, and G. Wotawa, "Validation of the Lagrangian particle dispersion model flexpart against large-scale tracer experiment data," Atmos. Environ. **32**, 4245–4264 (1998).
[4] T. S. Lundgren, "Turbulent pair dispersion and scalar diffusion," J. Fluid Mech. **111**, 27–57 (1981).
[5] G. Falkovich, K. Gawędzki, and M. Vergassola, "Particles and fields in fluid turbulence," Rev. Mod. Phys. **73**, 913–975 (2001).
[6] K. R. Sreenivasan and J. Schumacher, "Lagrangian views on turbulent mixing of passive scalars," Philos. Trans. R. Soc. A **368**, 1561–1577 (2010).
[7] B. L. Sawford, "Turbulent relative dispersion," Annu. Rev. Fluid Mech. **33**, 289–317 (2001).
[8] J. P. L. C. Salazar and L. R. Collins, "Two-particle dispersion in isotropic turbulent flows," Annu. Rev. Fluid Mech. **41**, 405–432 (2009).
[9] L. F. Richardson, "Atmospheric diffusion shown on a distance-neighbour graph," Proc. R. Soc. London A **110**, 709–737 (1926).
[10] A. S. Monin and A. M. Yaglom, *Statistical Fluid Mechanics* (MIT Press, Cambridge, MA, 1975), Vol. 2.
[11] M. C. Jullien, J. Paret, and P. Tabeling, "Richardson pair dispersion in two-dimensional turbulence," Phys. Rev. Lett. **82**, 2872 (1999).
[12] S. Ott and J. Mann, "An experimental investigation of the relative diffusion of particle pairs in three-dimensional turbulent flow," J. Fluid Mech. **422**, 207 (2000).
[13] N. Mordant, P. Metz, O. Michel, and J. F. Pinton, "Measurement of Lagrangian velocity in fully developed turbulence," Phys. Rev. Lett. **87**, 214501 (2001).
[14] F. Toschi and E. Bodenschatz, "Lagrangian properties of particles in turbulence," Annu. Rev. Fluid Mech. **41**, 375–404 (2009).
[15] M. Bourgoin, N. Ouellette, H. Xu, J. Berg, and E. Bodenschatz, "The role of pair dispersion in turbulent flow," Science **311**, 835–838 (2006).
[16] N. Ouellette, H. Xu, M. Bourgoin, and E. Bodenschatz, "An experimental study of turbulent relative dispersion models," New J. Turbul. **8**, 109 (2006).
[17] H. Xu, N. Ouellette, and E. Bodenschatz, "Evolution of geometric structures in intense turbulence," New J. Phys. **10**, 013012 (2008).
[18] B. Lüthi, S. Ott, J. Berg, and J. Mann, "Lagrangian multi-particle statistics," J. Turbul. **8**, N45 (2007).
[19] G. Boffetta and I. M. Sokolov, "Statistics of two-particle dispersion in two-dimensional turbulence," Phys. Fluids **14**, 3224 (2002).
[20] G. Boffetta and I. M. Sokolov, "Relative dispersion in fully developed turbulence: The Richardson's law and intermittency corrections," Phys. Rev. Lett. **88**, 094501 (2002).

[21] L. Biferale, G. Boffetta, A. Celani, B. J. Devenish, A. Lanotte, and F. Toschi, "Lagrangian statistics of particle pairs in homogeneous isotropic turbulence," Phys. Fluids **17**, 115101 (2005).
[22] J. F. Hackl, P. K. Yeung, and B. L. Sawford, "Multi-particle and tetrad statistics in numerical simulations of turbulent relative dispersion," Phys. Fluids **23**, 065103 (2011).
[23] J. Bec, L. Biferale, A. S. Lanotte, A. Scagliarini, and F. Toschi, "Turbulent pair dispersion of inertial particles," J. Fluid Mech. **645**, 497–528 (2010).
[24] M. van Aartrijk, H. J. H. Clercx, and K. B. Winters, "Single-particle, particle-pair, and multiparticle dispersion of fluid particles in forced stably stratified turbulence," Phys. Fluids **20**, 025104 (2008).
[25] J.-I. Choi, K. Yeo, and C. Lee, "Lagrangian statistics in turbulent channel flow," Phys. Fluids **16**, 779–793 (2004).
[26] R. H. Kraichnan, "Dispersion of particle pairs in homogeneous turbulence," Phys. Fluids **9**, 1937–1943 (1966).
[27] R. Scatamacchia, L. Biferale, and F. Toschi, "Extreme events in the dispersions of two neighboring particles under the influence of fluid turbulence," Phys. Rev. Lett. **109**, 144501 (2012).
[28] I. M. Janosi, P. Kiss, V. Homonnai, M. Pattantyus-Abraham, B. Gyure, and T. Tel, "Dynamics of passive tracers in the atmosphere: Laboratory experiments and numerical tests with reanalysis wind fields," Phys. Rev. E **82**, 046308 (2010).
[29] R. Bitane, H. Homann, and J. Bec, "Time scales of turbulent relative dispersion," Phys. Rev. E **86**, 045302 (2012).
[30] R. Bitane, H. Homann, and J. Bec, "Geometry and violent events in turbulent pair dispersion," J. Turbul. **14**, 23–45 (2013).
[31] F. T. M. Nieuwstadt and R. A. Brost, "The decay of convective turbulence," J. Atmos. Sci. **43**(6), 532–546 (1985).
[32] M. Antonelli, A. Lanotte, and A. Mazzino, "Anisotropies and universality of buoyancy-dominated turbulent fluctuations: A large-eddy simulation study," J. Atmos. Sci. **64**, 2642–2656 (2007).
[33] A. S. Lanotte and I. M. Mazzitelli, "Scalar turbulence in convective boundary layers by changing the entrainment flux," J. Atmos. Sci. **70**(1), 248–265 (2013).
[34] J. H. LaCasce, "Relative displacement probability distribution functions from balloons and drifters," J. Marine Res. **68**, 433–457 (2010).
[35] G. Lacorata, E. Aurell, B. Legras, and A. Vulpiani, "Evidence for a $k^{5/3}$ spectrum from the EOLE Lagrangian balloons in the low stratosphere," J. Atmos. Sci. **61**, 2936–2942 (2004).
[36] G. E. Willis and J. W. Deardorff, "A laboratory study of dispersion from an elevated source within a modeled convective planetary boundary layer," Atmos. Environ. **12**, 1305–1311 (1978).
[37] P. A. Durbin and J. C. R. Hunt, "Dispersion from elevated line sources in turbulent boundary layers," J. Méc. **19**, 679–695 (1980).
[38] F. T. M. Nieuwstadt, "A large-eddy simulation of a line source in a convective atmospheric boundary layer - I. Dispersion characteristics," Atmos. Environ. **26**, 485–495 (1992).
[39] P. Flohr and J. C. Vassilicos, "A scalar subgrid model with flow structure for large-eddy simulations of scalar variances," J. Fluid Mech. **407**, 315–349 (2000).
[40] A. Dosio and J. Vila-Guerau de Arellano, "Statistics of absolute and relative dispersion in the atmospheric convective boundary layer: A large-eddy simulation study," J. Atmos. Sci. **63**, 1253–1272 (2006).
[41] J. W. Deardorff, "Numerical investigation of neutral and unstable planetary boundary layers," J. Atmos. Sci. **29**, 91–115 (1972).
[42] J. W. Deardorff, "Three dimensional numerical study of the height and mean structure of a heated planetary boundary layer," Boundary-Layer Meteor. **7**, 199–226 (1974).
[43] C.-H. Moeng, "A large-eddy simulation model for the study of planetary boundary-layer turbulence," J. Atmos. Sci. **41**(13), 2052–2062 (1984).
[44] J. C. Wyngaard, "Large-eddy simulations: Guidelines for its application to planetary boundary layer research," U.S. Army Research Office Contract No. 0804, 1984.
[45] P. J. Mason, "Large eddy simulation of the convective atmospheric boundary layer," J. Atmos. Sci. **46**, 1492–1516 (1989).
[46] I. M. Mazzitelli, F. Toschi, and A. S. Lanotte, "An accurate and efficient Lagrangian sub-grid model," e-print arXiv:1402.4792 [physics.flu-dyn].
[47] M. Chertkov, A. Pumir, and B. I. Sharaiman, "Lagrangian tetrad dynamics and the phenomenology of turbulence," Phys. Fluids **11**, 2394 (1999).
[48] L. Biferale, G. Boffetta, A. Celani, B. J. Devenish, A. Lanotte, and F. Toschi, "Multiparticle dispersion in fully developed turbulence," Phys. Fluids **17**, 111701 (2005).
[49] B. J. Devenish and D. J. Thomson, "A Lagrangian stochastic model for tetrad dispersion," J. Turbul. **14**, 107–120 (2013).
[50] B. J. Devenish, "Geometrical properties of turbulent dispersion," Phys. Rev. Lett. **110**, 064504 (2013).
[51] M. Germano, U. Piomelli, P. Moin, and W. H. Cabot, "A dynamic subgrid-scale eddy viscosity model," Phys. Fluids **3**(7), 1760 (1991).
[52] U. Frisch, *Turbulence: The Legacy of A. N. Kolmogorov* (Cambridge University Press, 1995).
[53] E. Aurell, G. Boffetta, A. Crisanti, G. Paladin, and A. Vulpiani, "Growth of non-infinitesimal perturbations in turbulence," Phys. Rev. Lett. **77**, 1262–1265 (1996).
[54] E. Aurell, G. Boffetta, A. Crisanti, G. Paladin, and A. Vulpiani, "Predictability in the large: An extension of the concept of Lyapunov exponent," J. Phys. A **30**, 1–26 (1997).
[55] M. Cencini and A. Vulpiani, "Finite size Lyapunov exponent: Review on applications," J. Phys. A **46**, 254019 (2013).
[56] P. K. Yeung, S. B. Pope, and B. L. Sawford, "Reynolds number dependence of Lagrangian statistics in large numerical simulations of isotropic turbulence," J. Turbul. **7**, N58 (2006).
[57] A. S. Lanotte, L. Biferale, G. Boffetta, and F. Toschi, "A new assessment of the second order moment of Lagrangian velocity increments in turbulence," J. Turbul. **14**, 34–48 (2013).

[58] G. Gioia, G. Lacorata, E. P. Marques Filho, A. Mazzino, and U. Rizza, "The Richardson's law in large-eddy simulations of boundary layer flows," Boundary-Layer Meteor. **113**, 187–199 (2004).
[59] R. Ni and K. Q. Xia, "Experimental investigation of pair dispersion with small initial separation in convective turbulent flows," Phys. Rev. E **87**, 063006 (2013).
[60] J. Schumacher, "Lagrangian dispersion and heat transport in convective turbulence," Phys. Rev. Lett. **100**, 134502 (2008).
[61] P. K. Yeung and M. S. Borgas, "Relative dispersion in isotropic turbulence: Part 1. Direct numerical simulations and Reynolds number dependence," J. Fluid Mech. **503**, 93–124 (2004).